*Exploration Geophysics (2004) **35**, 25–32*
Butsuri-Tansa (Vol. 57, No. 1)
Mulli-Tamsa (Vol. 7, No. 1)

Seismic wave monitoring of CO_2 migration in water-saturated porous sandstone

Ziqiu Xue[1] **Takashi Ohsumi**

Key Words: P-wave velocity, strain, porous sandstone, monitoring, bedding plane, CO_2 sequestration

ABSTRACT

We have carried out laboratory measurements of P-wave velocity and deformation strain during CO_2 injection into a porous sandstone sample, in dry and water-saturated conditions. The rock sample was cylindrical, with the axis normal to the bedding plane, and fluid injection was performed from one end.

Using a piezoelectric transducer array system, we mapped fluid movement during injection of distilled water into dry sandstone, and of gaseous, liquid, and supercritical CO_2 into a water-saturated sample. The velocity changes caused by water injection ranged from 5.61 to 7.52%. The velocity changes caused by CO_2 injection are typically about -6%, and about -10% for injection of supercritical CO_2. Such changes in velocity show that the seismic method may be useful in mapping CO_2 movement in the subsurface.

Strain normal to the bedding plane was greater than strain parallel to the bedding plane during CO_2 injection; injection of supercritical CO_2 showed a particularly strong effect. Strain changes suggest the possibility of monitoring rock mass deformation by using borehole tiltmeters at geological sequestration sites. We also found differences associated with CO_2 phases in velocity and strain changes during injection.

INTRODUCTION

Carbon dioxide (CO_2) sequestration in geological formations is considered to be the most straightforward carbon management strategy for fossil-fuel-derived CO_2. The world's first commercial-scale CO_2 sequestration project is being operated by the Norwegian state oil and gas company Statoil in the North Sea. The CO_2 is an unwanted by-product of natural gas production from Sleipner West field. The CO_2 is injected into a large, deep, saline reservoir, the Utsira formation, 800 m below the bed of the North Sea (Baklid et al., 1996). The Sleipner project has suggested that an ideal site for CO_2 sequestration would be located in a geologically simple setting, with permeable reservoir rock, such as porous sandstone.

A major challenge in geological sequestration is to map the movement of CO_2 in the subsurface and to demonstrate that the CO_2 is safely contained within the reservoir. Recent research shows that seismic methods are among the most promising monitoring methods (Arts et al., 2002; Newmark et al., 2002; Hoversten et al., 2002). Seismic wave velocity is a function of mineralogical composition and porosity of the reservoir rock as well as fluid content and in-situ stress. When CO_2 is injected into an aquifer, the existing formation water in pore spaces of the reservoir rock will be partially displaced by the CO_2. This process will change the compressibility and density of the reservoir rock. These changes will in turn affect propagation characteristics of seismic waves. The effectiveness of seismic methods in monitoring CO_2 migration in an aquifer depends on the magnitude of seismic velocity changes caused by CO_2 injection. Previous field and laboratory studies have shown that compressional wave (P-wave) velocities were significantly decreased by CO_2 injection in porous sandstones (Wang and Nur, 1989; Xue et al., 2002).

In addition to a reduction of seismic wave velocity, CO_2 injection may cause a pore pressure increase in the subsurface, especially when the permeability of the reservoir rock is less than 20 millidarcy (van der Meer, 1992), because of the higher injection pressure of CO_2 compared to the pore pressure of the formation water. Wang et al. (1998) measured the pore pressure change in a CO_2-EOR (Enhanced Oil Recovery) field, and found a pore-pressure increase from 7.6 to 15.9 MPa due to the CO_2 flooding. This suggests that a field seismic survey would observe the combined effects of CO_2 saturation and pore pressure build-up. When interpreting the results of a field seismic survey, we need to evaluate the influence of pore pressure increase on seismic wave velocity and to compare it with the effect of CO_2 saturation. This paper describes an experimental study of P-wave velocity changes during the injection of gaseous, liquid, and supercritical CO_2 into water-saturated porous sandstone. This is a fundamental step toward understanding the effect of CO_2 injection on P-wave velocity in porous rocks. In this study, we also measured deformation strain in the sandstone sample during CO_2 injection. The strain measurements will be useful in the interpretation of rock mass deformation monitored by tiltmeter systems in large-scale injection sites.

EXPERIMENTAL PROCEDURE

A cylindrical sample of Tako sandstone (50 mm in diameter and 100 mm in length, 24% porosity) was used in this study. The sample was drilled normal to the bedding plane. Figure 1 shows the pore size distribution of Tako sandstone, measured by the mercury-injection method. Sixteen piezoelectric transducers with a characteristic frequency of 1 MHz, and six pairs of cross-strain gauges, were cemented to the sample surface (Figure 2). Grooved plates were attached to both ends of the sample. Concentric grooves connected by radial grooves were carved on the plate surface to ensure uniform injection over the entire surface of the sample. Stainless-steel end pieces were attached to both sample ends. The sample assembly was sealed with silicone sealant to prevent the invasion of oil, which was used as a hydrostatic pressure medium.

Two stainless-steel tubes were connected to the sample ends for pore-fluid injection. Pore fluids (distilled water and CO_2) were injected from the bottom of the sample. The ultrasonic pulse transmission technique was used to measure compressional wave (P-wave) velocity in this study. The waveform and strain data were monitored and recorded. In porous sandstones, P-wave velocity is strongly affected by closure of low-aspect-ratio

[1] *Research Institute of Innovative Technology for the Earth*
9–2 Kizugawadai, Kizu-cho, Soraku-gun,
Kyoto, 619-0292 JAPAN
Tel: +81-774-75-2312
Fax: +81-774-75-2313
Email: xue@rite.or.jp

Manuscript received July 14, 2003; accepted October 1, 2003. Part of this paper was presented at the 6th SEGJ International Symposium (2003).

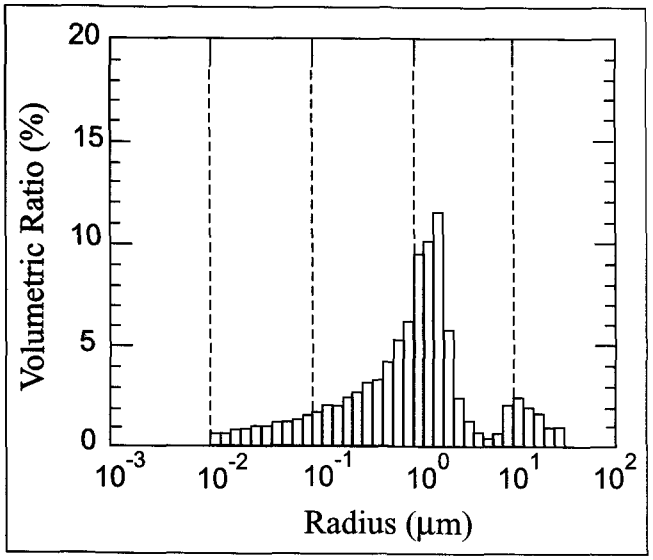

Fig. 1. Pore size distribution in Tako sandstone, obtained by the mercury-injection method (after Lin et al., 1997).

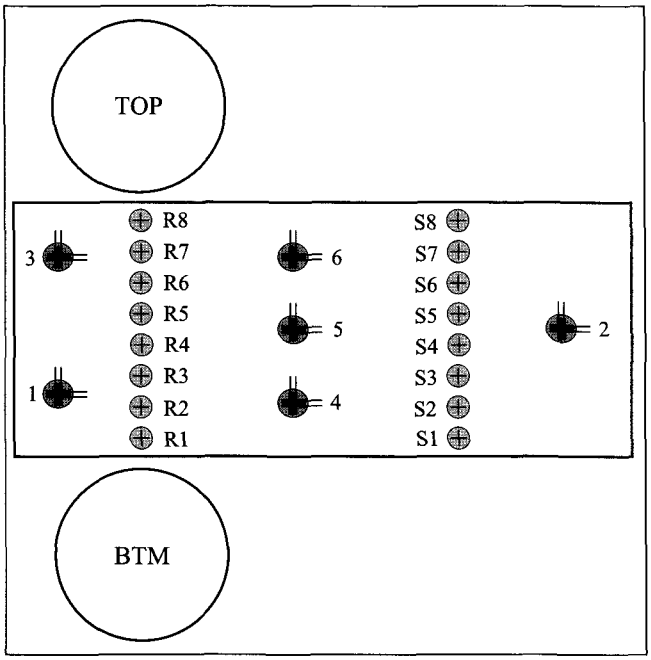

Fig. 2. Diagram of locations of piezoelectric transducers and strain gauges cemented to the sample. The diagram represents the cylindrical surface of the sample. Locations marked "S" are source transducers; locations marked "R" are receiver transducers, and the source and receiver transducers are diametrically opposite each other on the sample. P-wave velocities were measured along paths S1–R1, S2–R2, etc. Cross strain gauges for monitoring deformation associated with the CO_2 injection are identified by a single numeral.

micropores, and displacement of pre-existing pore water by injected CO_2 (Wilkens et al., 1986; Xue and Ohsumi, 2003). To eliminate the effects of low-aspect-ratio micropores on P-wave velocity, the dry sample was first subjected to hydrostatic pressure to 10 MPa. To examine the velocity variation caused by heterogeneity of the sandstone, P-wave velocity was measured along several different paths. Strain of the rock sample was measured simultaneously, to investigate the effect of bedding plane on deformation associated with CO_2 injection. After velocity and strain were measured in the dry sample, distilled water was injected into the dry sample at a constant pressure of 1 MPa. During water injection, P-wave velocities were measured along the eight paths connecting facing transducers (Figure 2) to monitor movement of injected water in the sample.

Figure 3 is a simplified diagram of the equipment. The CO_2 was injected from the bottom end of the sample at a constant pressure set by syringe pump A. Pore pressure was monitored at both ends of the sample. The pore pressure (back pressure) at the top end was kept constant by syringe pump B during CO_2 injection. Syringe pump B was set to reduce the pore pressure build-up caused by CO_2 injection. Syringe pump C was used to keep the hydrostatic pressure constant. By keeping constant pore pressure at both ends, and holding constant hydrostatic pressure, velocity changes caused by pore pressure build-up were minimised. Velocities and strains were measured for three different variations of physical conditions. The hydrostatic pressure, pressure at each end, and temperature conditions are shown in Table 1.

In case I, the sample was subjected to hydrostatic pressure of 10 MPa, and was saturated with water at a pore pressure of 3 MPa. Gaseous CO_2 was injected into the water-saturated sample at an injection pressure of 5 MPa and a temperature of 23°C. CO_2 injection was continued until P-wave velocities along all paths reached a new equilibrium state. After the gaseous CO_2 injection, the sample was flooded with fresh distilled water for several hours through syringe pump B, to remove the residual CO_2 in the sample. The pressure and temperature were then changed to the condition of case II in Table 1.

In case II, the hydrostatic pressure and pore pressure were 10 and 6 MPa, respectively. Liquid CO_2 was injected into the same sandstone sample at an injection pressure of 8 MPa and temperature of 23°C. Changes in P-wave velocity and strain were measured during the liquid CO_2 injection. After the liquid CO_2 injection, the sample was flooded with hot fresh water, and the pressure and temperature were changed to the case III conditions.

In case III (supercritical CO_2 injection) the pressure vessel was heated to 34°C by a controlled heating system. The syringe pump tanks A, B, and C, containing CO_2, pore water, and oil, respectively, were warmed by circulating water at 34°C. P-wave velocity and strain were measured in the same manner as for the gaseous and liquid CO_2 injections. In all the experiments, the same sample was used for examining effects of the CO_2 phases on velocity and strain. The flow rate of injected CO_2 depends on the permeability of the sample, and on pressure and temperature conditions.

CO_2 has a critical temperature and pressure of 31°C and 7.4 MPa. Above the critical point (Figure 4), CO_2 behaves like a gas, but it has a 'liquid' density that increases depending on pressure and temperature.

Case	Hydrostatic pressure(MPa)	Pore pressure(MPa)	CO_2 injection pressure(MPa)	Temperature of injected CO_2°C
I	10	3	5	23
II	10	6	8	23
III	15	10	12	34

Table 1. Pressure and temperature conditions for these experiments.

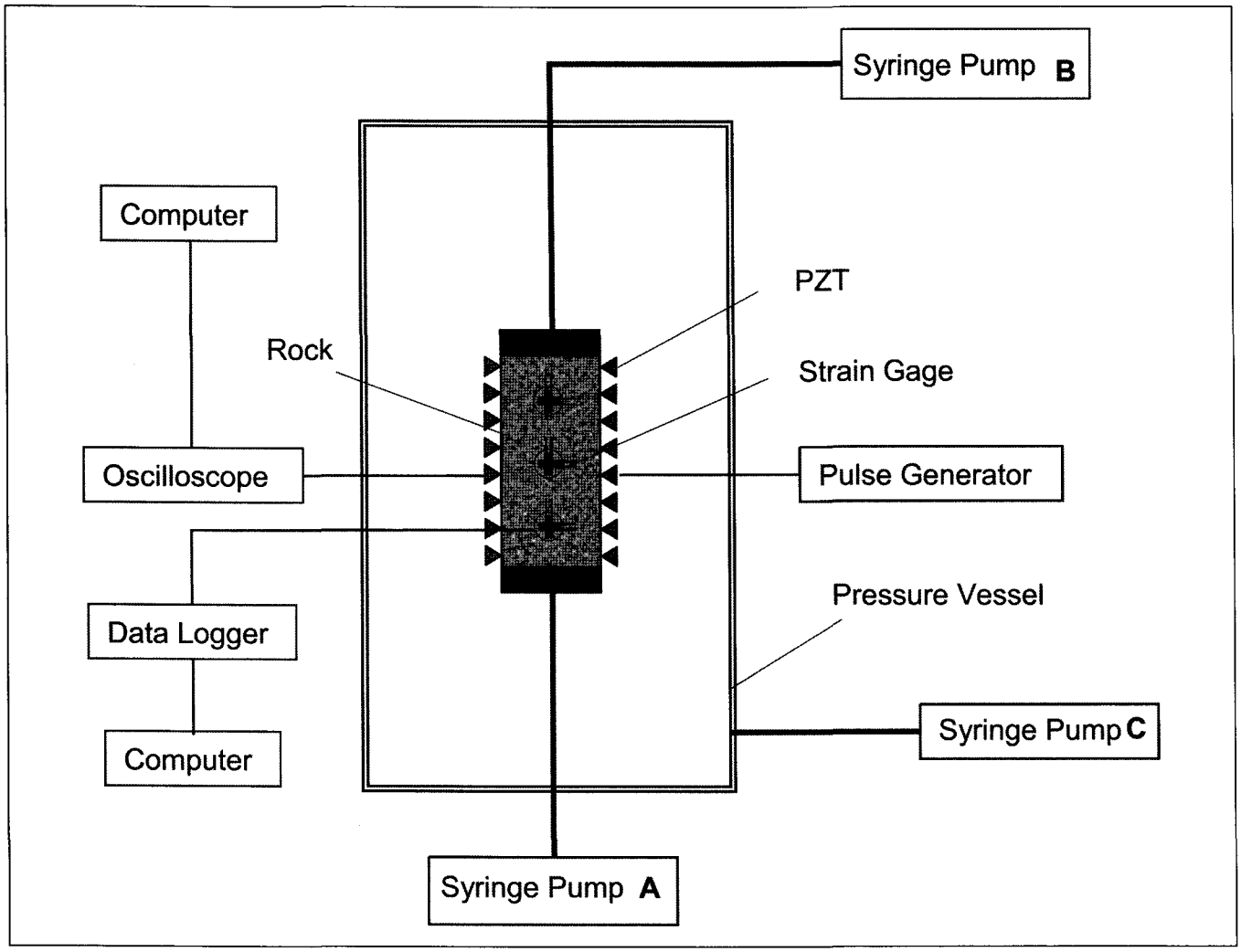

Fig. 3. Schematic layout of the experimental apparatus.

EXPERIMENTAL RESULTS

P-wave velocity changes caused by water injection in the dry sample

In the dry sample, P-wave velocities were measured along the 8 paths: S1–R1, S2–R2, S3–R3, S4–R4, S5–R5, S6–R6, S7–R7 and S8–R8. Those paths cross the sample axis and are parallel to the end surface of the sample (Figure 3). Figure 5 shows P-wave velocities along all paths as a function of hydrostatic pressure. As hydrostatic pressure increased, velocity along each path increased almost linearly. Velocity varied with path by about 10%, but the velocity change with change of hydrostatic pressure was less than this.

Distilled water was injected from the bottom of the sample at a constant pressure of 1 MPa. Figure 6 shows the P-wave velocity as a function of elapsed time for all paths during water injection. The velocities along paths S1–R1, S4–R4, S7–R7, and S8–R8 were interpolated by spline functions. Inflection points of velocity increase appeared in paths S1–R1, S4–R4, S7–R7 and S8–R8, in that order. The P-wave velocity along path S1–R1, located closest to the bottom of the sample, increased immediately after the commencement of water injection. The velocity increased appreciably, from the initial value of 3.46 km/s to a peak value of 3.65 km/s. P-wave velocity along the path S4–R4, located at the middle of the sample, began to increase at about 33 minutes after water injection commenced. About 100 minutes from the commencement of water injection, a velocity increase appeared along the path S7–R7. A velocity increase was observed along the

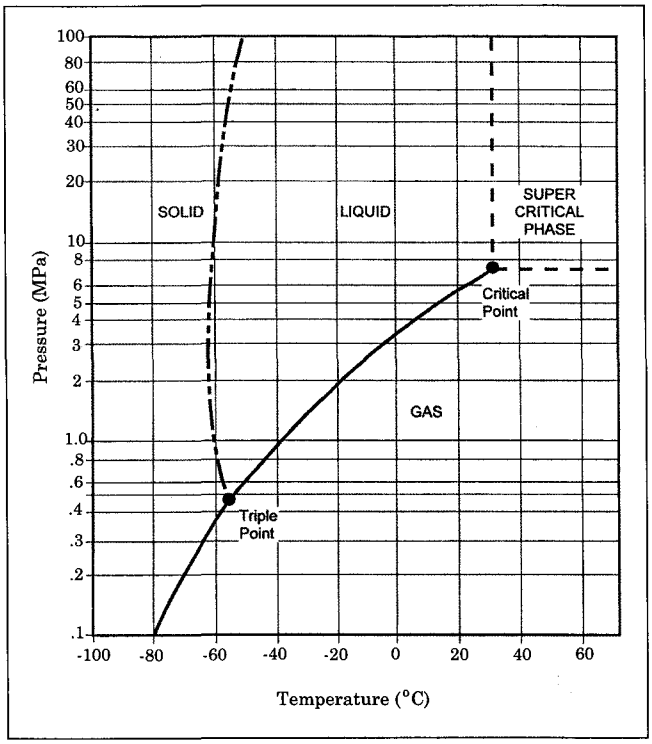

Fig. 4. Phase diagram for carbon dioxide.

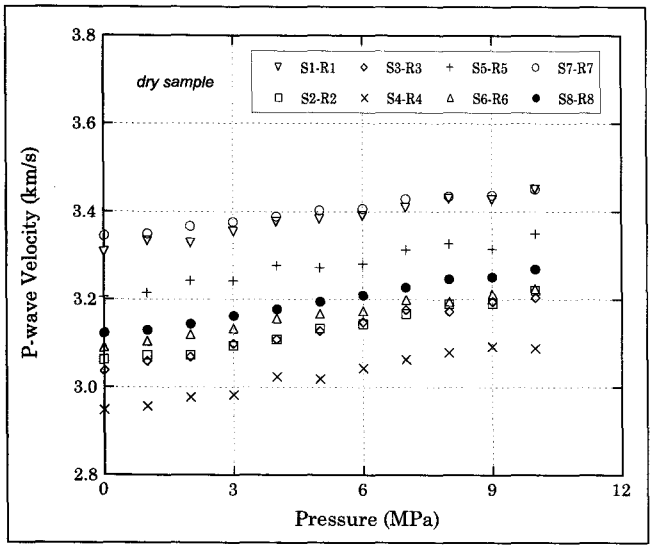

Fig. 5. P-wave velocities as a function of hydrostatic pressure in the dry sample.

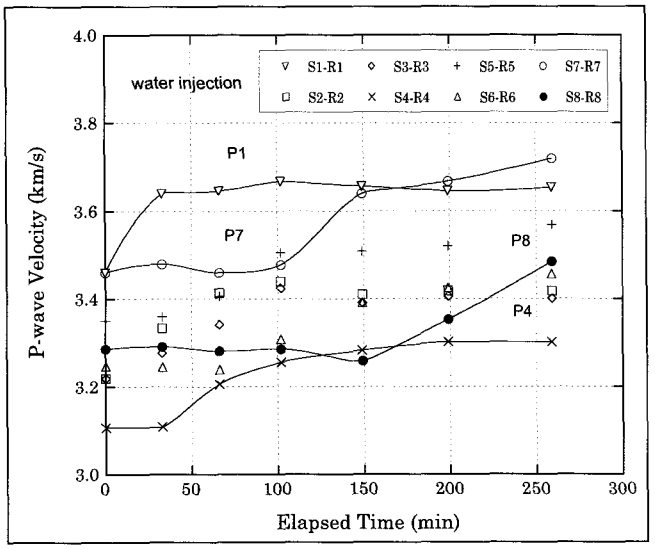

Fig. 6. P-wave velocity changes during water injection into the dry sample. Symbols refer to individual paths in the sample.

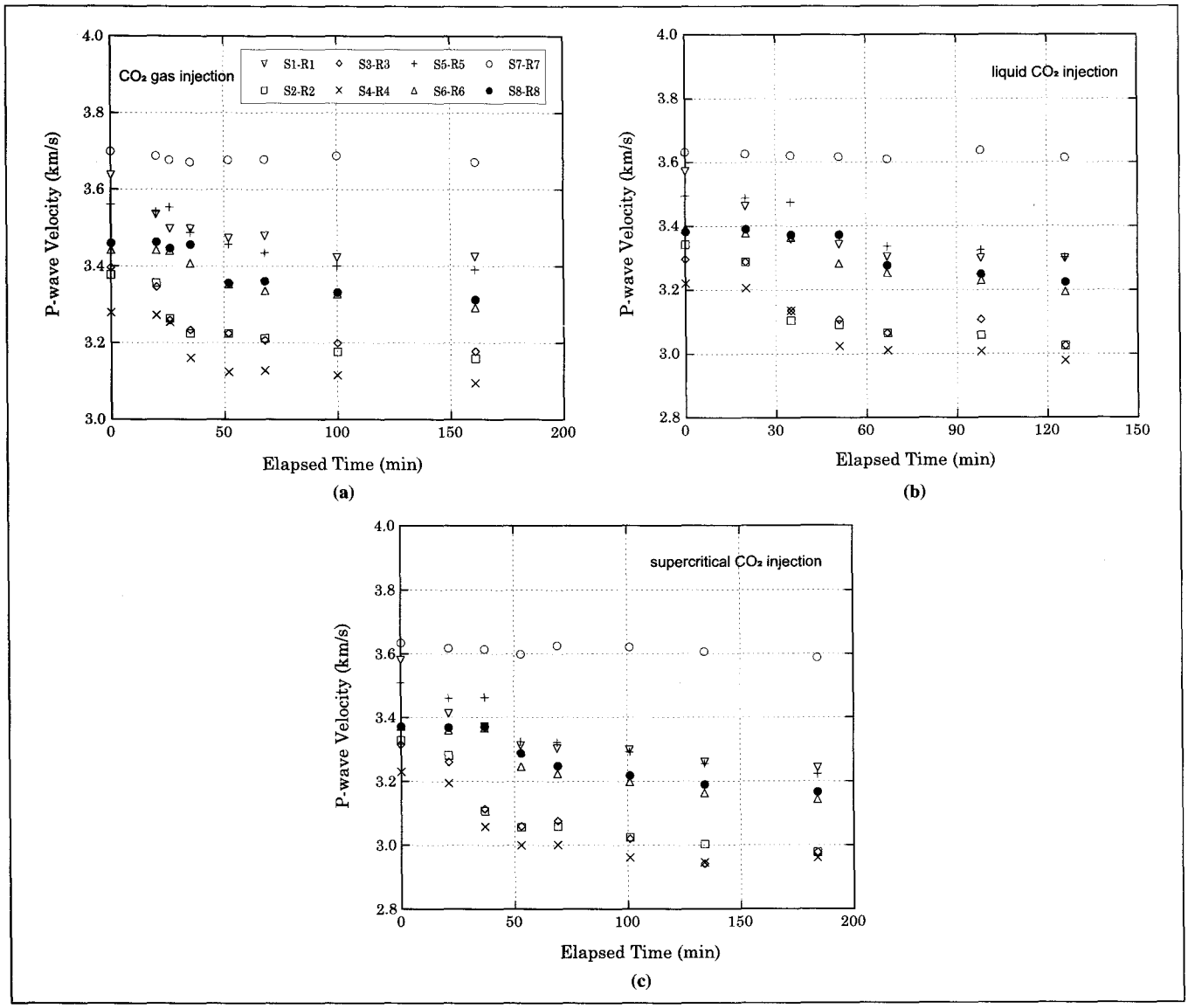

Fig. 7. P-wave velocity changes during CO_2 injection into the water-saturated sample. (a) gaseous CO_2 injection, (b) liquid CO_2 injection, (c) supercritical CO_2 injection. Symbols refer to individual paths in the sample: see Figure 7a for legend.

Case	S1–R1	S2–R2	S3–R3	S4–R4	S5–R5	S6–R6	S7–R7	S8–R8
I	-5.83	-6.46	-6.42	-5.61	-4.77	-4.36	-0.76	-4.25
II	-7.64	-9.48	-8.22	-7.51	-5.55	-5.84	-0.47	-4.70
III	-9.41	-10.57	-10.20	-8.36	-8.12	-6.76	-1.27	-6.08

Table 2. The percentage decrease in P-wave velocity during injection of gaseous, liquid, and supercritical CO_2 into the water-saturated sample. The headings refer to the source-receiver paths along which P-wave velocities were measured.

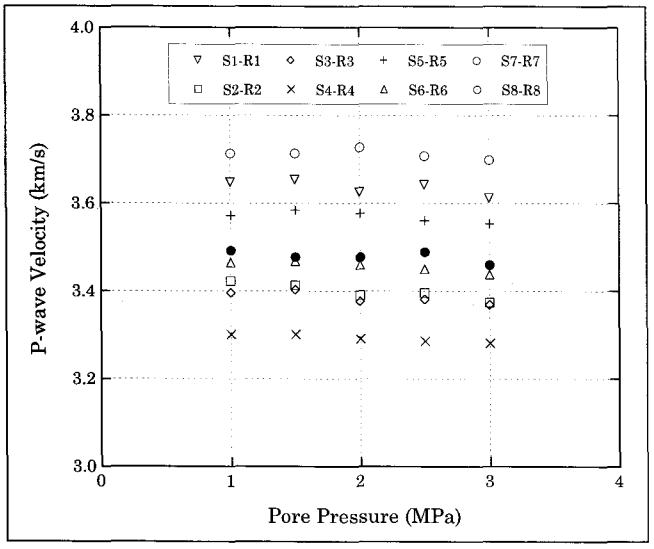

Fig. 8. P-wave velocity changes with respect to the pore pressure increase from 1 to 3MPa. The sample was subjected to a constant hydrostatic pressure of 10MPa. Symbols refer to individual paths in the sample.

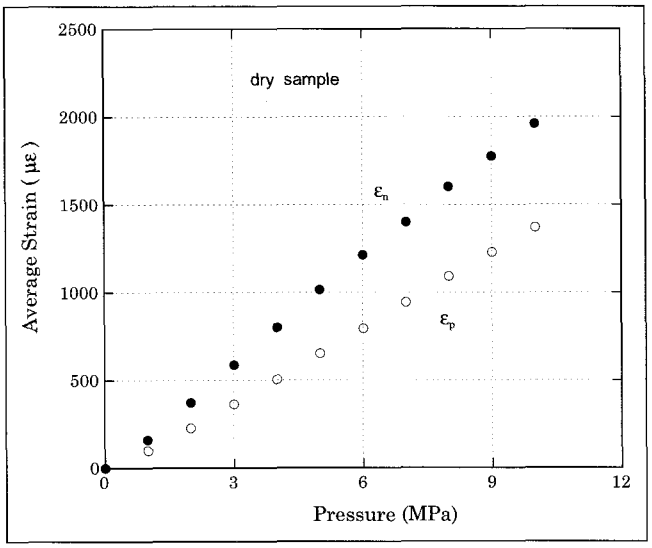

Fig. 9. Average strains as a function of hydrostatic pressure in dry sample. ε_n and ε_p indicate the strains measured normal and parallel to the bedding plane, respectively.

path S8–R8, which is located furthest from the bottom of the sample, at about 150 minutes after the water injection. The time lag between the paths S1–R1 and S8–R8 indicates the speed of fluid-front migration. The increase of P-wave velocity from the dry state to the saturated state ranged from 5.6 to 7.5%.

P-wave velocity changes caused by CO_2 injection in water-saturated sample

When injecting CO_2 into a water-saturated sample, pre-existing water within pore spaces will be partially displaced by CO_2. This process causes a reduction in P-wave velocity. In this study, three experiments were carried out to investigate the effects of CO_2 injection on P-wave velocity. Experimental conditions are shown in Table 1. In each case, the pressures of pore water and CO_2 were kept constant. The pore-water pressure was 2 MPa lower than the CO_2 injection pressure. Figures 7a, 7b, and 7c, respectively, show P-wave velocity changes during injections of gaseous, liquid, and supercritical CO_2 into water-saturated sandstone.

Figure 7a shows P-wave velocities during gaseous CO_2 injection. P-wave velocity along path S1–R1 decreased immediately after starting CO_2 injection. Velocities along paths S2–R2 and S3–R3 began to decrease about 20 minutes later. The velocity decrease moved upward, from the bottom to the top of the sample, although it was not detected on path S7–R7. A distinct decrease along the path S8–R8 (located closest to the top end of the sample) was observed about 35 minutes after commencement of gaseous CO_2 injection. At equilibrium, the velocity decrease ranged from 4.3 to 6.5% of the initial velocity.

Figure 7b shows the P-wave velocity observations during liquid CO_2 injection. Velocities along paths S1–R1 and S2–R2 decreased immediately after the CO_2 injection. Then P-wave velocity began to decrease in the following order: S3–R3 and S4–R4, S5–R5 and S6–R6, and S8–R8. P-wave velocity along path S7–R7 again showed a small change compared to other paths. The velocity along path S8–R8 began to decrease about 50 minutes after CO_2 injection began. The time lag of velocity decrease between the paths S1–R1 and S8–R8 was a little longer than that of gaseous CO_2 injection. When all velocities reached equilibrium states, the decrease ranged from 4.9 to 9.5%.

Figure 7c shows P-wave velocity change for supercritical CO_2 injection. Velocities along the paths S1–R1, S2–R2, S3–R3, S4–R4 and S5–R5 decreased almost simultaneously after CO_2 injection was begun. Velocities along paths S6–R6 and S8–R8 began to decrease about 37 minutes later. P-wave velocity along the path S7–R7 showed only a small change compared to other paths. The P-wave velocity decrease ranged from 6.1 to 10.6% when all velocities reached an equilibrium state. Thus, supercritical CO_2 injection resulted in the greatest reduction of velocity among the three injection experiments (Table 2).

Effects of pore pressure on P-wave velocity

While the sample was subjected to hydrostatic pressure of 10 MPa, P-wave velocity was measured with increasing pore pressure from 1 to 3 MPa, in steps of 0.5 MPa. P-wave velocity changes were also measured when the pore pressure was increased from 6 to 10 MPa, under the constant hydrostatic pressure of 15 MPa. Both experiments showed that the reduction of P-wave velocity was less than 2%. Figure 8 shows an example of effects of pore pressure on P-wave velocity in the sandstone. The results indicate that CO_2 injection causes larger velocity changes than those resulting from pore pressure changes.

Effects of bedding plane on strains

Six pairs of cross-strain gages were cemented on the sample in this study. Strains were measured along axial and circumferential directions. Those strains were used to calculate average strains

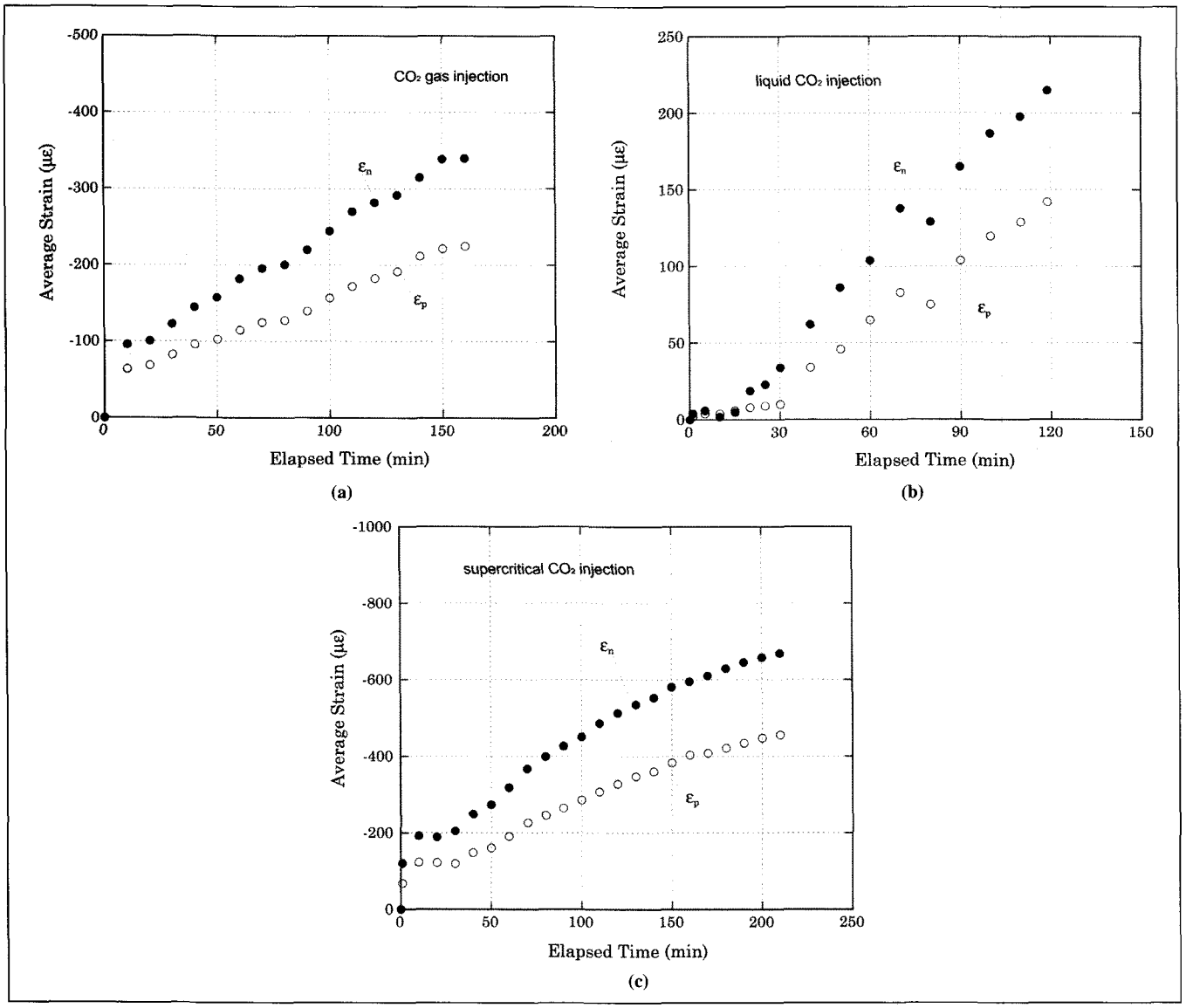

Fig. 10. Average strains as a function of time during CO_2 injection into the water-saturated sample. ε_n and ε_p indicate strains measured normal and parallel to the bedding plane, respectively. (a) gaseous CO_2 injection, (b) liquid CO_2 injection, (c) supercritical CO_2 injection.

that are normal and parallel to the bedding plane, ε_n and ε_p, respectively. Figure 9 shows ε_n and ε_p as a function of hydrostatic pressure in the dry sample. With increasing hydrostatic pressure, both ε_n and ε_p increased almost linearly up to 10 MPa. Throughout the entire experiment, ε_n was larger than ε_p, and the difference between the two strains became larger with increasing hydrostatic pressure, indicating that deformation along the bedding plane was predominant.

When gaseous CO_2 is injected into the water-saturated sample, ε_n and ε_p depend on elapsed time, as shown in Figure 10a. Both strains show a drastic change immediately after CO_2 injection is commenced. Ten minutes after injection commenced, ε_n and ε_p had decreased by about 30% of the total change. After this drastic decrease, both ε_n and ε_p decreased almost linearly with respect to elapsed time. The total decrease of average strain was 340 μ for ε_n and 220 μ for ε_p. Figure 10b shows the strain changes during liquid CO_2 injection. Both ε_n and ε_p decreased slightly in the first 15 minutes, then they decreased almost linearly, and showed a considerable decrease when injection was stopped. The total strain changes were 210 μ for ε_n and 140 μ for ε_p. In this case, the difference between two strains is similar to that in gaseous CO_2 injection, although the total decrease was smaller. Changes of ε_n and ε_p caused by supercritical CO_2 injection (Figure 10c) were very similar to those observed in gaseous CO_2 injection; the total decreases were 650 μ for ε_n and 420 μ for ε_p.

DISCUSSIONS AND CONCLUSIONS

P-wave velocity (V_p) in a homogeneous isotropic material is given by

$$V_p = \sqrt{\frac{K + (4/3)G}{\rho}}, \quad (1)$$

where K and G are the bulk and shear moduli, respectively, and ρ is the density of the material. The Gassmann equation gives the bulk modulus of the saturated porous rock (Gassmann, 1951):

$$K = K_d + \frac{(1 - K_d/K_s)^2}{\phi/K_f + (1-\phi)/K_s - K_d/K_s^2}, \quad (2)$$

where K, K_d, and K_s are the bulk moduli of the fluid-saturated and dry rock, and the solid framework of the rock, respectively. K_f is the modulus of pore fluid and ϕ is the porosity of the rock.

Sw	K_w (GPa)	1-S_w	Kc [1] (GPa)	Kf (GPa)	K (GPa)	ρ_c [2] (g/cm3)	ρ (g/cm3)	V_P (km/s)	$\Delta V/V_w$ [3] (% Calc)	$\Delta V/V_w$ [4] (% Obs)
Dry and water-saturated										
		P=10MPa	P_w=1MPa			T=23°C				5.6–7.5
0	2.25	1	0.006	0.006	11.013	0.001	1.905	3.214	dry	
1	2.25	0	0.006	2.250	15.395	0.124	2.135	3.357	saturated	
Gaseous CO_2 injection										
		P=10MPa	P_w=3MPa	P_{CO2}=5MPa		T=23°C				-4.3 – -6.5
0	2.25	1	0.006	0.006	11.013	0.124	1.934	3.190	-5.05	
0.2	2.25	0.8	0.006	0.007	11.016	0.124	1.974	3.158	-6.01	
0.3	2.25	0.7	0.006	0.009	11.019	0.124	1.994	3.142	-6.48	
Liquid CO_2 injection										
		P=10MPa	P_w=6MPa	P_{CO2}=8MPa		T=23°C				-4.9 – -9.5
0	2.25	1	0.066	0.066	11.144	0.7	2.066	3.097	-7.89	
0.2	2.25	0.8	0.066	0.082	11.179	0.7	2.080	3.089	-8.12	
0.3	2.25	0.7	0.066	0.093	11.203	0.7	2.087	3.086	-8.21	
Supercritical CO_2 injection										
		P=15MPa	P_w=10MPa	P_{CO2}=12MPa		T=34°C				-6.1 – -10.6
0	2.25	1	0.046	0.046	11.101	0.623	2.048	3.107	-7.70	
0.2	2.25	0.8	0.046	0.057	11.125	0.623	2.066	3.095	-8.03	
0.3	2.25	0.7	0.046	0.065	11.142	0.623	2.074	3.090	-8.18	
0.7	2.25	0.3	0.046	0.146	11.319	0.623	2.109	3.078	-8.53	

[1] Wang (2000)
[2] Marden (1976)
[3] the percentage decrease in P-wave velocity from the water-saturated state due to CO_2 saturation, by Gassmann's theory
[4] experimental data, this study

Table 3. Physical properties of rock and fluids used for calculating P-wave velocities, based on Gassmann's theory. Velocities were calculated for different degrees of water saturation, and the calculated change in velocity is compared with the experimental data on change in velocity, given in the final column.

The shear modulus G of the rock is not affected by fluid saturation;

$$G = G_d , \tag{3}$$

where G_d is the shear modulus of the rock. The density ρ of the saturated rock is simply given by

$$\rho = \rho_d + \phi \rho_f , \tag{4}$$

where ρ and ρ_d are the fluid-saturated and dry densities of the rock, respectively, and ρ_f is the fluid density in the pores.

When injecting CO_2 into the water-saturated sample, some CO_2 is dissolved in the water but the amount of dissolved CO_2 is unknown. We consider the fluid to be a mixture of pure water and pure CO_2. The bulk modulus K_f of the water/CO_2 mixture inside the pore spaces can be calculated using Wood's equation (Wood, 1941)

$$\frac{1}{K_f} = \frac{S_w}{K_w} + \frac{1-S_w}{K_c} , \tag{5}$$

where K_w and K_c are the bulk moduli of water and CO_2, respectively. S_w is the fraction of water in the fluid filling the pores (the saturation). The bulk density ρ_f of the water/CO_2 mixture is calculated by

$$\rho_f = S_w \rho_w + (1-S_w)\rho_c , \tag{6}$$

where ρ_w and ρ_c are the bulk densities of water and CO_2, respectively.

Here we compare the measured P-wave velocity in dry sample with the values predicted by the Gassmann equation. The framework bulk modulus of Tako sandstone was chosen as an average of the bulk modulus of quartz and feldspar; K_s = 38 GPa (Wang, 2000). The shear modulus was given by an experimental study: G = 6.5 GPa (Lin et al., 1997). The dry density was measured in this study: ρ_d = 1905 kg/m^3. Table 3 shows results calculated for velocity change in the present experiments: (1) from dry to water saturation, (2) gaseous CO_2 injection into water-saturated rock, (3) liquid CO_2 injection into water-saturated rock, and (4) supercritical CO_2 injection into water-saturated rock.

Effects of water and CO_2 saturation on P-wave velocity

When water is injected into the dry sample, pore spaces are filled with water. The P-wave velocity becomes larger than that in the dry state, because of the increase of fluid bulk modulus in the pores. The change of P-wave velocity due to water saturation ranged from 5.6 to 7.5% (Figure 6). However, the calculated velocity increase was about 4.5%, lower than the measured value (Table 3). This difference can be interpreted as the effect of pore geometry on P-wave velocity. Kuster and Toksöz (1974) demonstrated that flat pores have much more effect on P-wave velocity change than spherical pores with an equal porosity. They concluded that even at a very low porosity (e.g., 0.01%) flat pores affect P-wave velocity change by 10% or more, during water saturation. Figure 1 shows the pore-size distribution of the Tako sandstone. Pores with radius of the order of 0.01 mm may be considered to be flat pores, so they very much affect the P-wave velocity change.

After injection of CO_2, the sample is partially saturated with water and partially saturated with CO_2. Since we did not measure the amount of residual water or injected CO_2 in the sample, we have assumed several different values for the water and CO_2 fractions.

We calculated the P-wave velocity as a function of water saturation, S_w. The bulk modulus of the gaseous CO_2-saturated sample (K) is comparable to that of dry sample for S_w = 0 - 0.3 (Table 3, case I). The overall density is larger than the dry sample, because of the replacement of air with water. This results in a P-wave velocity that is smaller than that in the dry state. For the liquid-CO_2 injection case (Table 3, case II), both the overall density and the bulk modulus are larger than that after gaseous-CO_2 injection. However, the velocity decrease is larger than after gaseous-CO_2 injection. This indicates that the increase in density affects the velocity more than the change of bulk modulus does. For supercritical-CO_2 injection (Table 3, case III), both the bulk modulus and the density are lower than that after liquid-CO_2 injection. The velocities for different saturations S_w are almost the same as after liquid-CO_2 injection.

By comparing the calculated P-wave velocity change with the present experimental data on CO_2 injection, the observed velocity changes show fairly good agreement with the calculated values, although the experimental data are distributed over a considerable range. The trend of velocity changes from gaseous, liquid, and supercritical CO_2 injection can be successfully modelled by the Gassmann equation if the slight difference caused by flat pores is ignored.

It is also notable that the present experimental results show a wide distribution of the velocity change during CO_2 injection. This suggests that migration of CO_2 in the rock sample is not homogeneous. Inhomogeneous pore distribution or inhomogeneous distribution of fluid flow channels may cause inhomogeneous CO_2 migration.

Application to seismic survey and tilt measurements in CO_2 monitoring

Underground CO_2 sequestration is expected to target aquifers deeper than 800 m. Seismic methods are expected to be promising tools for monitoring the state of CO_2 in the aquifer. Considering the pressure and temperature conditions of such an aquifer, a supercritical phase is expected for CO_2 in the deep aquifer. The present experimental results show that P-wave velocity is appreciably decreased, from 6.1% to 10.6%, by supercritical CO_2 injection. This suggests that the movement of injected CO_2 in the aquifer may be detectable by either cross-well or high-resolution surface seismic methods, because the McElroy data suggests that high-resolution cross-well tomography can resolve a 1% velocity change (Harris et al., 1995).

Wang et al. (1998) showed that a P-wave velocity decrease in a field survey was the result of the combined effects of CO_2 saturation and pore pressure build-up. The pore pressure build-up strongly depends on the permeability of the reservoir rocks (van der Meer, 1992). To separate the effect in field seismic data caused by pore pressure build-up, S-wave velocity or electromagnetic measurements will be required (Wang et al., 1998; Hoversten et al., 2002). In this study we also measured the P-wave velocity decrease with increasing pore pressure, and found that the effect of pore pressure increase was much smaller than that caused by CO_2 saturation. Therefore, we may be able to distinguish the velocity change caused by CO_2 saturation from the velocity change caused by pore pressure build-up.

Vasco et al. (2001) successfully applied tilt measurements and borehole pressure data to image a high-permeability channel within a shallow fracture zone in a geothermal field. The present experimental results indicate that strains are reduced during CO_2 injection. The strain changes with respect to elapsed time after CO_2 injection are considered to result from the replacement of pore water with injected CO_2. As the injected CO_2 migrates through pore spaces, effective stress is reduced locally, and strain became smaller because of the reduction in local effective stress. Strains measured normal to the bedding plane were more affected than those measured parallel to the bedding plane, especially in the case of supercritical CO_2 injection. Such strain changes suggest the possibility of monitoring a CO_2-bearing aquifer by the deformation of the rock mass.

ACKNOWLEDGEMENTS

We thank Osamu Sano and Kin'ichiro Kusunose for their thoughtful review comments, which have helped substantially to improve this paper. One of the authors, Z. Xue, expresses deep gratitude to Osamu Nishizawa for his encouragement and support in this study. This work was supported by the Ministry of Economy, Trade, and Industry of Japan under the contract: "Research and Development of Underground Storage Technology for Carbon Dioxide".

REFERENCES

Arts, R., Eiken, O., Chadwick, A., Zweigel, P., van der Meer, L., and Zinszner, B., 2002, Monitoring of CO_2 injected at Sleipner using time lapse seismic data: in Gale and Kaya (eds.), *Proc. 6th International Conference on Greenhouse Gas Control Technologies (GHGT6)*, 347–352.

Baklid, A., Korbol, R. and Owren, G., 1996, Sleipner west CO_2 disposal, CO_2 injection into a shallow underground aquifer: *Proceedings – SPE Annual Technical Conference and Exhibition*, 269–277.

Gassmann, F., 1951, Ueber die Elastizität poröser Medien: *Vieteljahrsschrift der Naturforschenden Ges., Zurich*, **96**, 1–23.

Medard, L.A., 1976, *Gas Encyclopaedia*: Elsevier.

Harris, J.M., Nolen-Hoeksema, R.C., Van Schaack, M., Lazaratos, S.K., and Rector, J.W., 1995, High-resolution crosswell imaging of a west Texas carbonate reservoir: Part I-Project summary and interpretation: *Geophysics*, **60**, 667–681

Hoversten, G., Gritto, R., Daley, T., Majer, E., and Myer L., 2002, Crosswell seismic and electromagnetic monitoring of CO_2 sequestration: in Gale and Kaya (eds.), *Proc. 6th International Conference on Greenhouse Gas Control Technologies (GHGT6)*, 371–376.

Lin, W. Nakamura, T. and Fujita, M., 1997, Variation of ultrasonic wave amplitude in Inada granite and Tako sandstone under triaxial compression process: *32nd Japanese National Conference on Geotechnical Engineering*, 1249–1250.

Newmark, R., Ramirez, A., and Daily, W., 2002, Monitoring carbon dioxide sequestration using electrical resistance tomography (ERT): A minimally invasive method: in Gale and Kaya (eds.), *Proc. 6th International Conference on Greenhouse Gas Control Technologies (GHGT6)*, 353–358

Kuster, G.T., and Toksöz, M.N., 1974, Velocity and attenuation of seismic waves in two-phase media: Part I, Theoretical Formulations: *Geophysics*, **39**, 587–606.

Vasco, D.W., Karasaki, K., and Kishida, K, 2001, A coupled inversion of pressure and surface displacement: *Water Resources Research*, **37**, 3071–3089.

van der Meer, L., 1992, Investigations regarding the storage of carbon dioxide in aquifers in the Netherlands: *Energy Convers. Mgmt.* **33**, 611–618.

Wang, Z., 2000, The Gassmann equation revisited: comparing laboratory data with Gassmann's predictions: in Wang and Nur (eds.), *Seismic and Acoustic Velocities in Reservoir Rocks, Volume 3, Recent Developments*, 8–23.

Wang, Z., and Nur, A., 1989, Effects of CO_2 flooding on wave velocities in rocks with hydrocarbons: *Society of Petroleum Engineers, Reservoir Engineering*, **3**, 429–439.

Wang, Z., Cates, M., and Langan, R., 1998, Seismic monitoring of a CO2 flooding in a carbonate reservoir: A rock physics study: *Geophysics*, **63**, 1604–1617

Wilkens, R.H., Simmons, G., Wissler, T.M., and Caruso, L., 1986, The physical properties of a set of sandstones, Part III, The effects of fine-grained pore-filling material on compressional wave velocity: *Int. J. Rock Mech. Min. Sci & Geomech. Abstr.*, **23**, 313–325.

Wood, A.B., 1941, *A textbook of sound*: G. Bell and Sons.

Xue, Z., Ohsumi, T., and Koide, H., 2002, Laboratory measurements of seismic wave velocity by CO_2 injection in two porous sandstones: in Gale and Kaya (eds.), *Proc. 6th International Conference on Greenhouse Gas Control Technologies (GHGT6)*, 359–364.

Xue, Z., and Ohsumi, T., 2003, Laboratory measurements on gas permeability and P-wave velocity in two porous sandstones during CO_2 flooding: *Journal of the Mining and Material Processing Institute of Japan*, (in press).